Přírodovědecká fakulta
Faculty of Science

Jihočeská univerzita v Českých Budějovicích
University of South Bohemia in České Budějovice

Isolation, purification and characterization of bacteriochlorophyll c for engineering of novel photonic materials

Bachelor Thesis

Institute of Chemistry

Submitted by: Matin Kazemi

Supervisor: Mgr. David Kaftan, PhD.

Co-Supervisor: Ing. David Kahoun, PhD.

České Budějovice, Czech Republic 2019

Kazemi, M., 2019: Isolation, purification and characterization of bacteriochlorophyll c for engineering of novel photonic materials. BSc. Thesis, in English; Faculty of Science, University of South Bohemia in České Budějovice, Czech Republic.

Annotation: Optimization of efficient pigment extraction from thermophilic green non-sulfur photosynthetic bacterium *Chloroflexus aurantiacus* was achieved. Method for purification of the extracted pigments was optimized using several types of high-performance liquid chromatography columns and gradient and isocratic elution protocols. Purity of the obtained bacteriochlorophyll c was validated in mass spectrometer. Aggregates of purified bacteriochlorophyll c molecules were prepared by conventional methods and imaged in atomic force microscope.

Declaration of Academic Honesty

I hereby declare to have worked and written this Bachelor Thesis on my own. All additional sources are listed in the bibliography section. Furthermore, I declare that, in accordance with Article 47b of Act No. 111/1998 in the valid wording, I agree with the publication of my bachelor thesis, in full form in the Faculty of Science archive, in electronic form in publicly accessible part of the STAG database operated by the University of South Bohemia in České Budějovice accessible through its web pages. Further, I agree to the electronic publication of the comments of my supervisor and thesis opponents and the record of the proceedings and results of the thesis defense in accordance with aforementioned Act No. 111/1998. I also agree to the comparison of the text of my thesis with the Theses.cz thesis database operated by the National Registry of University Theses and a plagiarism detection system.

České Budějovice, December 2019

……

Matin Kazemi

Acknowledgement

I would first like to express the deepest appreciation to my thesis advisor Dr. David Kaftan of the Institute of Chemistry at the Faculty of Science of the University of South Bohemia. Also, I would like to thank my co-supervisor Dr. David Kahoun of the Institute of Chemistry at the Faculty of Science of the University of South Bohemia

I must express my very profound gratitude to my parents and my husband for providing me with unfailing support and continuous encouragement throughout my years of study. Thank you.

Abstract

Bacteriochlorophyll c is one of the photosynthetic pigments present in the light-harvesting complexes of green non-sulfur photosynthetic bacterium *Chloroflexus aurantiacus*. Inside the cells, molecules of bacteriochlorophyll c self-assemble into densely packed aggregates that exhibit exceptional excitonic coupling among the individual pigments. Utilization of the unique properties of these pigment aggregates in industrial applications requires understanding of their structure. To this end, preparation of artificial aggregates constructed using chemically pure constituents is an indispensable prerequisite for the determination of their structure. In this work, an efficient method for bacteriochlorophyll c extraction from *Chloroflexus aurantiacus* cells was developed. The procedure requires additional step of extraction that enhances bacteriochlorophyll c yields over the less polar pigments. Next, rapid and cost effective pigment purification method of isocratic HPLC was optimized yielding highly pure fraction of bacteriochlorophyll c. The method protocol allows pigment separation in under 10 minutes utilizing Kinetex C18 chromatographic column washed by a single solvent – methanol. The method validity and bacteriochlorophyll c purity was confirmed by LC-MS.

Table of Contents

3-Hydroxypropionate	**3HOP**
AFM	Atomic Force Microscopy
APCI	Atomic pressure chemical ionization
BChl	Bacteriochlorophyll
***Cba*.**	*Chlorobaculum*
C. phaeovibriodies	*Chlorobium phaobacteroids*
Cfl.	*Chloroflexus*
Chl	Chlorophyll
HOPG	Highly ordered pyrolytic graphite
HPLC	High-performance liquid chromatography
LC	Liquid chromatography
LED	Light emitting diode
MS	Mass spectrometry
MeOH	Methanol
PDA	Photodiode array detection
QI	Quantitative imaging
SNL	Sharp nitride lever
SPD	Spectrophotometric detector
SPM	Scanning probe microscopy
STM	Scanning tunneling microscopy
UV-VIS	Ultraviolet-Visible

1. Introduction

1.1. Photonic materials

The photonics are widely considered as instrumental in every aspect of human effort [1]. Photonic material also known as optical materials are a class of electromagnetic meta materials interacting with light [2]. They together with the instruments are essential elements regarding information processing, telecommunications, solar cells, chemical sensors, magneto-optic memories, light emitting diodes, color imaging, video systems and other key utilizations [3]. The scopes in the field of photonic materials is wide and accounts for the emerging synthetic bio-photonic, polymer materials and extends furthermore to the subfields of the well-established glass and semi-conductor materials [2]. Moreover, Advances of photonic materials resulted in prominent achievements allowing regulation of light-matter interaction and flow of light through light trapping in thin films for solar cell applications, also control of the photonic crystal processing, understanding the various applications of nano-photonic light, controlling the flow of light optical meta-materials [2, 3]. The materials are extremely diverse and are based on combination of science of materials. Almost all materials in any form has been embedded in photonic and electronic materials [3]. Furthermore, bio-inspired photonic materials are in fact artificial materials with optical characteristics as inspiration of structures found in the living organisms [4,5]. The structures of synthetic optical materials may constitute replicas of natural optical structure or may be based on design principles which are adapted by nature to achieve the desired properties [4]. In contrast, the other important aspect of synthetic photonic materials structures is that they can exhibit electric and magnetic properties which are not found in natural materials [6]. The main interest of photosynthetic materials is testing of bioinspired materials for feasibility in industrial applications (e.g. organic photovoltaics).

1.2. Chlorophylls and bacteriochlorophylls

Chlorophylls and bacteriochlorophylls play essential role in light energy capturing and photochemical energy conversion in processes of photosynthesis. Chlorophyll molecule comprises of two different parts: a long hydrocarbon tail and a porphyrin head. The latter is simply defined as four pyrrole rings with nitrogen coordinating magnesium ion in most Chls and BChls. except in *Acidiphilium rubrum* which coordinates Zn ion [7]. One of the main distinctions among different types of chlorophylls (Chls) and bacteriochlorophylls (BChls) that define specific spectral properties, is the level of macrocycle unsaturation [8]. A completely unsaturated phyto-porphyrin macrocycle in the c-type Chls of chromophyte algae has a typically strong absorption in the blue spectral region (Soret or B-bands, $\varepsilon \approx 150{,}000$) and just a moderate absorption in the zone ~620 nm (Qy-bands $\varepsilon \approx 20{,}000$). The phytochlorin type is a 17,18-trans-dihydro-phytoporphyrin represented by the Chl a, b, and d that are synthetized by the organisms performing oxygenic photosynthesis whereas BChl c, d, and e are found in the green anoxygenic photosynthetic bacteria (Fig. 1). In organic solvents, such pigments have absorption bands at approximately 440 and 660 nm of the same intensity ($\varepsilon \approx 100{,}000$) with an apparent gap in the green spectral zone. It is clear that in a specific manner, the Chls general nomenclature has no relationship with their degree of

unsaturation. It would not show their origin because the bacteriochlorophylls involve phytochlorins and bacteriochlorins whereas cyanobacteria utilize a similar phytochlorin type Chls, which the green plants have [9].

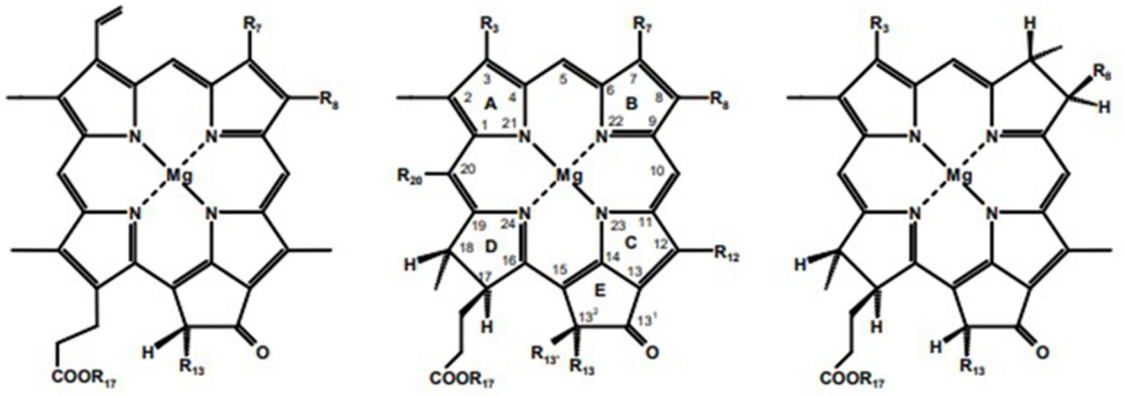

Pigment	R_3	R_7	R_8	R_{12}	$R_{13'}$	R_{13}	R_{17}	R_{20}	Macrocycle
Chl a	C_2H_3	CH_3	C_2H_5	CH_3	H	$COOCH_3$	Phy	H	Chlorin
Chl b	C_2H_3	CHO	C_2H_5	CH_3	H	$COOCH_3$	Phy	H	Chlorin
Chl d	CHO	CH_3	C_2H_5	CH_3	H	$COOCH_3$	Phy	H	Chlorin
Phe a	C_2H_3	CH_3	C_2H_5	CH_3	H	$COOCH_3$	Phy	H	Chlorin
BChl c	$CHOH-CH_3$	CH_3	C_2H_5	CH_3/C_2H_5	H	H	Far + others	CH_3	Chlorin
BChl d	$CHOH-CH_3$	CH_3	C_2H_5	CH_3/C_2H_5	H	H	Far + others	H	Chlorin
BChl e	$CHOH-CH_3$	CH_3	C_2H_5	CH_3/C_2H_5	H	H	Far + others	CH_3	Bacteriochlorin
BChl a	$CO-CH_3$	CH_3	C_2H_5	CH_3	H	$COOCH_3$	Phy	H	Bacteriochlorin
BChl b	$CO-CH_3$	CH_3	$=CH-CH_2$	CH_3	H	$COOCH_3$	Phy	H	Bacteriochlorin
BChl g	$CO-CH_3$	CHO	$=CH-CH_2$	CH_3	H	$COOCH_3$	Phy	H	Bacteriochlorin
BPhe a	$CO-CH_3$	CH_3	C_2H_5	CH_3	H	$COOCH_3$	Phy	H	Bacteriochlorin
Chl(ide) c_1	C_2H_3	CH_3	C_2H_5	CH_3	H	$COOCH_3$	$H^{a,b)}$	H	Porphyrin
Chl(ide) c_2	C_2H_3	CH_3	C_2H_3	CH_3	H	$COOCH_3$	$H^{a,b)}$	H	Porphyrin
Chl(ide) c_3	C_2H_3	$COOCH_3$	C_2H_5	CH_3	H	$COOCH_3$	$H^{a,b)}$	H	Porphyrin
[8-Vinyl]-PChlide a	C_2H_3	CH_3	C_2H_5	CH_3	H	$COOCH_3$	$H^{a,b)}$	H	Porphyrin

Figure 1. Bacterio chlorin-type Chls (single-bonds between C7/C8 & C-17/C-18 in left) and phyto-porphyrin-type Chls (in the right).Numbering is based on IUPAC-IUB [9].

1.2.1. Bacteriochlorophyll c

BChl c is a photosynthetic pigment that is a crucial constituent of the light harvesting antennae of green sulfur and non-sulfur photosynthetic bacteria (Fig. 2) [10]. The molecules of BChl c self-assemble into rod-shaped structures called chlorosomes recognized by the increased efficiency of the energy transfer [11, 12]. Qy (0–0) transition of BChl c emerges at 660–670 nm in the polar solvents, in which the BChl c is found as a monomer, whereas Qy (0–0) BChl c transition in chlorosomes would be highly red-shifted to 740–750 nm [13, 14]. Absorption spectra of chlorosomes are very similar to the spectra of the aggregated BChl c generated in non-polar

solvents [13, 15]. In addition to the 740 nm aggregates, BChl c generates multiple intermediate aggregates, all of which show a distinct Qy (0–0) absorption maximum [15- 18]. For instance, BChl 230 c would form '680 nm aggregates' and '710 nm aggregates', whose Qy (0–0) transitions are found around 680 nm and 710 nm, respectively, when dichloromethane (CH_2C_{l2}) titration dissociates the 740 nm aggregates in hexane [10, 15]. Other studies used absorption [14], infrared (IR) [19], circular dichroism (CD) [13, 19], resonance Raman, and 1H-nuclear magnetic resonance (NMR) measurement to examine BChl c aggregation. Stability of the 680 nm, 710 nm, and 740 nm aggregates is dependent both on the temperature and pigment concentration and on the chiral structure at the 31-position and the solvent nature [20, 21]. Consequently, in the case of the investigation of the equilibrium and aggregation structures, it is necessary to consider the effects of stereochemistry and the solvent feature [19]. Green sulfur photosynthetic bacteria (*Chlorobiaceae*) produce a remarkable abundance of BChl pigments which are primarily used as light harvesting antennae. In the case of the green bacteria, two different BChls have been identified designated as the BChls c and d. Brockmann and co-workers have recently characterized two new BChls [21]. BChl e was identified in *Chlorobium phaeobacteroides* while compound closely related to BChl c (compound lf), was found in the green non sulfur filamentous bacterium *Chloroflexus (Cfl.) aurantiacus*. The latter type differs from BChl c only in the nature of the esterifying alcohol. The major esterifying alcohol in the BChls c and d is farnesol [21].

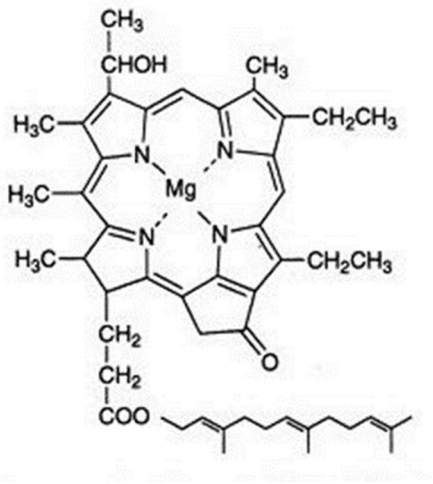

Figure 2. Molecular structure of the bacterio-chlorophyll c (BChl c) [22].

1.2.2. Natural BChl c aggregate - chlorosome

The green non-sulfur filamentous anoxygenic phototrophic bacterium *Cfl. aurantiacus* [23, 24] harbors one of the most efficient light harvesting system known to science. The light harvesting complex composed of self-assembled BChl c called chlorosome [25, 26] is bound to the inside of the cytoplasmic membrane via a pigment-protein structure known as baseplate. This antenna channels energy of the captured light to a chimeric photosystem with common features with the green sulfur bacteria and purple photosynthetic bacteria. This B808-866 light harvesting core complex [26] encloses the quinone type (or type-II) reaction center [27, 28] placed into the

cytoplasmic membrane. The BChl a containing light harvesting complex B806-866 shows an approximately 10-fold lower absorbance at 866 nm in comparison to the BChl c containing chlorosomes at 740 nm when the cells are grown under low light intensity and anaerobic conditions [23, 25]. Therefore, chlorosomes contribute crucially to the capability of the green bacteria to perform photosynthesis under very low light conditions [28-30]. It is widely accepted that chlorosomes consist of BChl c, d, and e molecules (BChl f has been observed in the *Chlorobaculum limnaeumm* mutants) [28, 31].

The pigments making up the chlorosome self-aggregate without involvement of the peptides in a hydrophobic context containing a lipid monolayer [32, 33-35]. Chlorosomes also contain very different proteins in comparison with other photosynthetic antennae. The most abundant CsmA protein forms the baseplate pigment-binding protein, which acts as the energy mediator from BChl c in chlorosome and BChl a in the integral light harvesting complexes [29, 36]. Spectroscopic, microscopic and molecular modeling approaches were employed for investigation of supramolecular nanostructures of chlorosomes [32] revealing rod and or lamellar nanostructures of BChls [32, 37-38]. Natural aggregates of BChl c (chlorosomes) were inspected by the freeze fracture scanning electron microscopy in *Cfl. aurantiacus* ok-70-fl and detected as the rods with a 5 nm diameter. One of the other studies demonstrated that chlorosomal BChls are the magnesium complexes of 31-hydroxy 131-oxo chlorins. Numerous molecular variants were observed in the *Cfl. aurantiacus* chlorosomes [32]. Such chlorosomes contain 8-ethyl-12-methyl- BChls c having different hydro-carbon chains at the 17-propionate residue: stearyl (C18), R17 = cetyl (C16), phytyl (C20), oleyl (C18), and geranylgeranyl groups (C20). The above BChls c are an epimeric mix at the chiral 31-position so that (31R)/(31S) ratio has been 2/1 in *Cfl. aurantiacus*. Hence, BChls c from *Cfl. aurantiacus* were known as R/S [E, M] BChl-c. The first R/S shows 31-stereo-chemistry and the terms in brackets represent 12-methyl (M) and 8-ethyl (E) groups [19, 20, 30, 32]. Central BChl's magnesium and peripheral 31-hydroxy and 131-oxo substituents are the prerequisite for their self-aggregation in a chlorosome.

1.2.3. *Chloroflexus aurantiacus*

The cells of *Cfl. aurantiacus* were first observed in the Hakone district in an isolated hot spring near Sokokura in Japan (Tab. I) [29]. The type strain *Cfl. aurantiacus* J-10-fl lives in a microbial mat with cyanobacteria in a Yellowstone National Park. Its specific physiology demonstrates its unique position in the evolution of photosynthesis [29] exhibiting growth as an anaerobic phototroph, whereas it grows as an aerobic chemotroph in the dark. *Cfl. aurantiacus* utilizes organic carbon sources such as lactate, acetate, butyrate, propionate produced by the related cyanobacteria in the *Chloroflexus*/cyanobacterial mats of its natural habitat. Moreover, it can use a 3-hydroxypropionate (3HOP) autotrophic carbon fixation cycle to assimilate CO_2 [39- 40]. No considerable differences in the cell dimension or shape in the cells grown phototrophically and aerobically were shown [41]. However, other studies did not observe any differentiation of the cytoplasmic membrane during the formation process of photosynthetic apparatus [42, 43].

Table I. Organism data on the *Chloroflexus aurantiacus* [29].

Organism Data	
Organism name	***Chloroflexus aurantiacus***
Lineage	Bacteria; Chloroflexi, Chloroflexi, Chloroflexaceae, Chloroflexales, Aurantiacus, Chloroflexus.
Oxygen requirement	Facultative aerobe, anaerobe.
Habitat	Fresh water, hot springs.
Motility	Motile
Temperature optimum	Thermophile (52-60°C)
Cell shape	Filaments
Cell arrangement	Filaments
Gram staining	Gram-negative
Phenotype	Green non-sulfur
Energy source	Light (phototroph) and organic carbon sources (chemotroph).
Carbon assimilation	Photo-autotrophy, photo-heterotrophy, chemo-heterotrophy.

2. Goals

The aims of the work are:

1. Maintenance and growth of pure cultures of *Chloroflexus aurantiacus* on a medium scale for production of raw pigment material.
2. Optimization of high yield extraction of bacteriochlorophyll c into organic solvents.
3. Optimization of efficient separation technique using HPLC and its implementation for obtaining highly purified bacteriochlorophyll c.
4. Preparation of bacteriochlorophyll c aggregates.
5. Immobilization and imaging of bacteriochlorophyll c aggregates using AFM.

3. Materials and Methods

3.1. Cell growth

The source of pigments for all experiments was a strain of a thermophilic filamentous green non-sulfur bacterium *Cfl. aurantiacus* [23] that was isolated from a sample originally collected in a hot spring in Rupite, Bulgaria [43]. Cells were grown in a half strength of liquid R2A medium [44] (Tab. II) with full formulation of vitamins (Tab. III) and trace elements (Tab. IV) in 250 mL glass bottles and on solidified ½ R2A medium solidified by 1.5% agar on petri dishes. Cell cultures were grown in an incubator that kept constant temperature of 50°C. Agar plates were passaged on the weekly basis in a sterile hood. The batch liquid cultures were transferred into flasks of a larger volume every week. Fresh medium was always added in a sterile hood. Finally, the cell culture was transferred into 1 L glass bottle. The cell cultures were illuminated by light emitting diode (LED) illumination panel providing white light of 50 μmol photons m^{-2} s^{-1}. Aeration was provided by continued bubbling via sterile air and stirring using magnetic stirrer (<150 rpm). Fresh medium was added frequently to compensate for nutrient consumption and water evaporation. After week of growing the culture aerobically, the batch culture of *Clf. aurantiacus* was cultivated at 50 °C anaerobically for another week to stimulate production of BChl c. Lowering the concentration of oxygen inside the culture medium was achieved by bubbling by sterile nitrogen gas. The 1 L bottle containing the cell culture was closed quickly with a screw cap afterwards, leaving minimal gas phase above the culture medium.

Table II. R2A medium composition.

R2A Medium	
Yeast extract	0.50 g
Proteose peptone	0.50 g
Casamino acids	0.50 g
Glucose	0.50 g
Soluble starch	0.50 g
Na-pyruvate	0.30 g
K_2HPO_4	0.30 g
$MgSO_4 \times 7\ H_2O$	0.05 g
Agar	15.00 g
Distilled water	1000.00 mL

Table III. Vitamin solution composition.

Vitamin solution	
p-Aminobenzoate	1.00 mg
Biotin	0.20 mg
Nicotinic acid	2.00 mg
Thiamine-HCl × 2 H_2O	1.00 mg
Ca-pantothenate	0.50 mg
Pyridoxamine	5.00 mg
Vitamin B_{12}	2.00 mg
Distilled water	100.00 mL

Table IV. Trace element solutions SL-4 and SL-6 composition.

Trace element sol. SL-4	
EDTA	0.50 g
$FeSO_4$ × 7 H_2O	0.20 g
Trace element sol. SL-6	100.00 mL
Distilled water	900.00 mL
Trace element sol. SL-6	
$ZnSO_4$ × 7 H_2O	0.10 g
$MnCl_2$ × 4 H_2O	0.03 g
H_3BO_3	0.30 g
$CoCl_2$ × 6 H_2O	0.20 g
$CuCl_2$ × 2 H_2O	0.01 g
$NiCl_2$ × 6 H_2O	0.02 g
$NaMoO_4$ × 2 H_2O	0.03 g
Distilled water	1000.00 mL

3.2. Pigment extraction

Anaerobically grown cells of *Cfl. aurantiacus* were aliquoted into 50 mL centrifugation tubes and were harvested by centrifugation at 14000 rpm at 4°C for 10 minutes. The combined pellets were homogenized by a glass piston homogenizer. Homogenized cells were transferred into a clean tube containing glass beads and an extraction buffer composed of mixture of acetone: methanol: 50 mM Tris, pH 8 (7:2:1, v/v/v). Pigments were extracted by vortexing the homogenized pellet with beads in the extraction buffer at room temperature in the dark for 15 minutes. The cells debris containing unextracted pigments was separated from the supernatant containing the extracted pigments by centrifugation. The resultant supernatant was passed though PVDF filter of 0.2 µm

pore size using clean glass syringe. The pigment extract was vacuum dried in a rotary evaporator and resuspended in a pure methanol. Aliquots of the pigment extract pipetted into 2 mL amber vials were blown with sterile nitrogen to remove oxygen. Samples were then stored and at -20°C until final processing.

3.2.1. BChl c aggregates preparation

The HPLC purified BChl c dried in stream of pure nitrogen gas was resuspended in small volume of dichloromethane. Hexane was added to the solution by ratio (10:1) forming BChl c aggregates for AFM imaging.

3.3. HPLC

High performance liquid chromatography or High-pressure liquid chromatography (HPLC) is a method of column chromatography well suited for analyses and separation, identification, and quantification of chemical mixtures (Fig. 3) [45]. A chromatographic column is used in HPLC to hold a packaging substance (the stationary phase), while a pump moves a mobile phase(s) across the column. The detector registers the analyzed molecules employing measurements of absorbance, pH, conductivity or other means including light scattering. The time of a given analyte eluting (exiting the column's end) is called the retention time. The retention time varies according to interaction established between the stationary phase, the molecules under examination, and the solvent(s) that involve(s) miscible combination of water or organic solvents. Methanol and acetonitrile are the most common solvents found in mobile phase formulations. A small volume of an examined specimen is carried by the mobile phase. Variation of the mobile phase compositions over the analyte separation is called gradient elution in contrast to the isocratic elution by constant formulation of the mobile phase. The choice of the solvents, additives, and gradients is dictated by the physicochemical properties of the stationary phase and analyte [46].

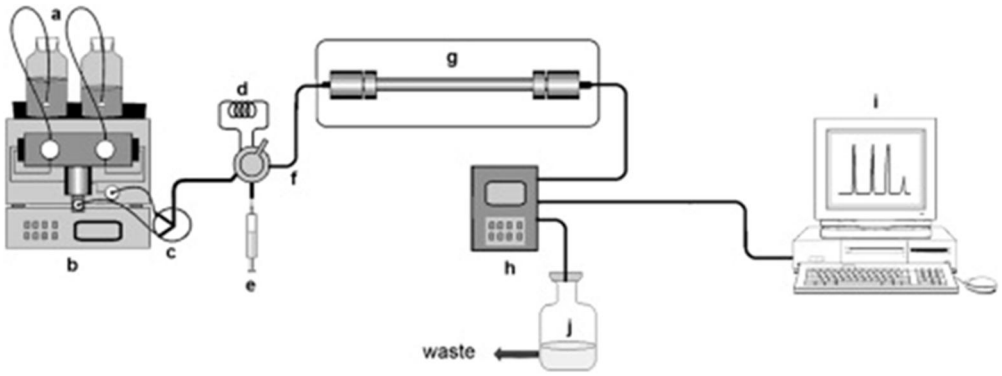

Figure 3. Diagram of a HPLC: a. solvents (mobile phases), b. high pressure pump, c. mixer for the homogenization of the mobile phases, d. sample loop, e. syringe with sample, f. injector valve, g. oven with HPLC column, h. detector, i. data system (procedure & register), & j. the collection vial [47].

Normal-phase chromatography is used for separation of polar compound by both polar stationary phase and a nonpolar mobile phase. Whereas, reversed-phase chromatography is commonly used for separation of compound with hydrophobic moieties which lack a dominant polar characteristic (regardless of polarity of the compound). In RP-HPLC, the stationary phase is hydrophobic and the mobile phase is either polar or partially polar and is used with bonded phase (hydrocarbon chain; C8, C18) on silica. The mobile phase is composed of two phase solvent (aqueous and organic phases) and is higher in polarity than the stationary phase [48].

The high-performance liquid chromatography (HPLC) was used to separate the extracted pigments using various reverse phase columns in HPLC Prominence system (Shimadzu) equipped with manual injection valve, dual wavelength SPD-20A detector and a fraction collector. Four reverse phase HPLC columns were used. First of the columns used was Kinetex C-8 (2.6µm, 30×2.1mm, Phenomenex), the flow rate was 0.45 mL/min, the pressure was 18 MPa. The second column used was Jupiter C-5 (5µm, 300 Å, 170 sq. m/g, Phenomenex), the flow rate and the pressure were 4 mL/min and 18 MPa respectively. Third column used was Luna C8 (3 µm, 100 Å, 440 sq. m/g, Phenomenex). The flow rate and the pressure were 3mL/min and 16 MPa respectively. The injection volume was 10µL for C8-Kinetex and 20µL for C5-Jupiter and C8-Luna. All samples were injected manually. Absorbance of the eluted peaks was graphically recorded at wavelengths corresponding to the short wavelength absorption maxima of each pigment: at 438 and 671 nm for C-8, at 441 and 674 nm for column C-5 and at 440 nm and 672 nm for column C8-luna. Mobile phases included two mixtures solvents. Solvent mixture A was composed of methanol: 28mM ammonium acetate + water (70:30). Solvent B was methanol. All solvents were of MS grade. A gradient of these solvent mixtures was used during the total run time of 35.01 minutes according to Table V.

Table V. Gradient of mobile phases.

Time	%A	%B
0.00	100.0	0.0
4.00	0.0	100.0
18.00	0.0	100.0
21.00	0.0	100.0
24.00	0.0	100.0
31.00	100.0	0.0
35.01	100.0	0.0

The final results were obtained with a Kinetex EVO C18 column (150×4.6 mm, 2.6 µm, 100 Å, Phenomenex). Twenty µL of analyte was eluted isocratically with 100% methanol at a rate of 1 mL/min at pressure of 18MPa. BChl c was monitored at 668 nm. Eluted fractions per 0.5 mL were collected by a fraction collector.

3.4. Mass Spectrometry (MS)

Mass spectrometry is one of the vacuum techniques, which provides, separates, and detects the mass ions (the ratio of mass to charge) from the intended molecules. It possesses several kinds of configurations and platforms for diverse utilizations. Mass spectrometry is usually having an interface with gas chromatography (electron ionization/chemical ionization source) and liquid chromatography (electrospray or atmospheric pressure chemical ionization) for analyzing the cellular elements (biomarkers) [49]. Liquid chromatography mass spectrometry (LC-MS) is one of the analytical techniques utilized in recognizing the elements in chemical mixtures. In this method, a chemical mix enters a liquid chromatograph in its simplest form, in which partial or complete separation occurs in the respective component segments. Then, elution of such different components can be observed from the liquid chromatograph in discrete sequence over time. Afterwards, the liquid chromatograph effluent enters a mass spectrometer, in which the mass spectra will be obtained from the separated components. At the end, the mass spectra achieved by this method can be clarified for determining the molecular weights and molecular structures for diverse components [50].

Purification of the pigment extract from *Cfl. aurantiacus* was performed using isocratic elution (100% methanol) on Kinetex C18 column. Efficiency of this purification step was evaluated using LC-PDA-APCI-MS/MS technique under identical chromatographic conditions including the identical HPLC column. Extract sample was analyzed before and after the purification step. Differences in obtained chromatograms (PDA detection), full scan MS spectra of precursor ions in the peak of interest and full scan MS/MS spectra of product ions from target compound (BChl c) were assessed qualitatively.

3.5. UV-VIS Spectroscopy

UV-VIS spectroscopy is one of the absorption spectroscopy techniques, which is suited for analysis of a specimen containing species absorbing light in ultraviolet to visible range. The absorption is a mere manifestation of the excitation of the chemical species from its ground state to an excited one. The less energy is necessary for this transition, the higher is the numerical value of the absorption wavelength [51].

Light passing a solution containing a colored substance is attenuated because the dye molecules absorbed the photons. The Lambert Beer's Law formulates the relation of the amount of the light eliminated because of absorption and the concentrations of the absorbing materials. With given incident light intensity I_0, molar absorptivity coefficient ε, molar concentration c of the absorbing material, and the path length the beam travels across the solution, changes in the light intensity caused by the absorption are:

$$dI = I_0 - \varepsilon\, c\, dx$$

The integration over the path length x, returns $I/I_0 = e^{-\varepsilon c x}$ a parameter known as Transmittance, T. Nonetheless, the amounts of the light absorbed by a material in solution is most often represented by Absorbance, A:

$$A = \text{Log}\,(I_0 / I) = \varepsilon\, c\, x$$

The absorbance has thus a linear relationship to the molar absorptivity ε with units of mol^{-1} cm^{-1}, the sample path length in cm, x, and the compound concentration in the solution written in mol L^{-1}, c. Actually, molar absorptivity ε is one of the measures of the amounts of the light absorbed in each unit concentration. In fact, it is a constant for a specific material substance and the applied wavelength.

The absorption spectra of samples obtained from high performance liquid chromatography were measured by a UV-VIS spectrophotometer (Lambda 35, Perkin Elmer, USA). One hundred of µL of sample were diluted in 500 µL of methanol and the sample was placed into a quartz cuvette. A fast scan was used in the range of 400-800 nm.

3.6. Atomic Force Microscopy (AFM)

Atomic Force Microscopy (AFM) represents the most popular scanning probe technique among the local scanning probe microscopy (SPM). AFM has an ability to image a surface with atomic resolution in the real time which provide the ground for studying atomic structure of the surface and identify the location of separate point defects and absorbs. The fundamental principle of the AFM relies on measurements of local attractive or repulsive forces acting between atomically sharp tip and sample. These forces are monitored by a bending, or deflection, of the cantilever. A majority of the AFMs employ a 4 quadrants photo-diode for registering the cantilever bending. AFM is specifically suited for biological research since it is possible to image the samples under physiological conditions. It is not necessary to stain or coat the sample that also does not need to be conductive. Hence, high resolution imaging is attainable in a physiological buffer or medium under wide range of temperatures. Additional to the 3D topography data, AFM measurement provides information about mechanical features or adhesion [52]. AFM operating in non-contact mode measures local forces deriving from the chemical bonds formation and breaking between the outermost tip-apex atoms and surface atoms. During this measurement mode the AFM tip is brought into oscillation at a short distance above the surface of the sample. An atomic-scale contrast in the AFM images can be considered as a convolution of geometric characteristics of the surface and a “chemical” contribution. The magnitude of the forces leading to an atom-resolved non-contact AFM imaging are dependent on the tip-apex atoms affinity for interacting with certain surface atoms. Current research envisions a high potential in the concurrent AFM/STM imaging [53, 54].

Specialized imaging modes of AFM, such as the quantitative imaging (QI) mode reveal surface topography of the sample under minimum load of force. The QI mode of AFM collects data along force-distance curves at each pixel in a high-resolution image ensuring a control over the forces

exerted between the tip and the sample's surface. Such a multi-parametric mode generates force curves with data of the surface stiffness, adhesion, and height at every high-resolution pixel. In addition, lack of the lateral forces allows for imaging of soft biological and loosely bound samples like bacterial aggregates.

AFM imaging of BChl c aggregates was performed using NanoWizard 4 BioScience AFM (Bruker Inc., USA) atop of IX73P2F inverted optical microscope (Olympus, Japan). The AFM system was placed on Halcyonics i4LARGE active vibration isolation system (Accurion GmbH, Germany) inside the custom-made acoustic enclosure. Standard scanner on a manual sample stage were used. The sample was adsorbed over the freshly cleaved highly-ordered pyrolytic graphite (HOPG). BChl c aggregates were imaged in air using Fastscan-B probe (Bruker Inc., USA) having a spring constant of k = 1.15 $N.m^{-1}$ and resonant frequency of fo = 224.1 kHz. Imaging in a buffer (Tris 50 mM, pH 7.8, 100 mM NaCl) was achieved using B cantilever of a SNL-10 probe (Bruker Inc., USA) with the spring constant of k = 0.124 $N.m^{-1}$ and resonant frequency fo = 4.87 kHz. All imaging was performed at 23˚C. Images of 256 x 256 μm^2 (1x1 μm^2) were recorded with resolution of 256 x 256 $pixels^2$ using Quantitative Imaging (QI) mode (1.5 µm Z range, 41.7 µm/s tip horizontal speed). Thermal noise, contact-based method of cantilever spring constant calibration was performed using formalism of Hutter and Bechhoeffer [55].

4. Results

4.1. Growth of *Chloroflexus aurantiacus* cells

The cell cultures of *Cfl. aurantiacus* were maintained on agar (Fig. 4) in an incubator at 50˚C under low light intensity of 10-20 µmol photons m^{-2} s^{-1}. Orange, filamentous, irregular colonies were observed on agar plates (Fig. 4). The cells scraped from the agar plate by sterile spatula was inoculated into the liquid ½ R2A medium. Liquid cultures were grown in an incubator at 50˚C at light of 50 µmol photons m^{-2} s^{-1}. The brown filamentous cultures were observed in liquid medium. Gentle aeration provided mixing of the culture along with the magnetic stirrer. The culture appeared homogeneous and orange in color. Under anaerobic conditions, filaments usually adhered to the side of the vessel nearest the light during the final stage of cell growth. Stirring with the magnetic fish then became critical for even nutrient distribution in the batch culture that was not mixed by air bubbling during the final phase of anaerobic growth.

Figure 4. Cell culture of *Chloroflexus auraniacus* on agar plates.

4.2. Extraction of BChl c from cells

Extraction of BChl c from cells of *Cfl. aurantiacus* cells was performed by harvesting the cells with centrifuge and homogenizing the pellets by glass piston homogenizer. For extracting pigments from pelleted cells 7:2:1 (v/v/v) Acetone/Methanol/Tris solvent mixture was used. After removing cell debris by centrifuging, the supernatant was filtered and transferred to rotary evaporator to dry. Further, the pigment extract was resuspended into pure methanol and blew it with nitrogen. Finally, the sample is ready for next approaches.

4.3. High Pressure Liquid Chromatography (HPLC) purification of BChl c pigments

HPLC chromatogram of the pigment extract separation using C5-Jupiter column (0.4mL/min flow, 18MPa pressure, 20µl of sample injected) is shown in Fig.5. There are two main elution peaks appearing at retention times of 25 and 27 min (Fig. 5a). The second major peak was collected and its absorption spectrum measured (Fig. 5b). A strong absorption peak dominated the spectrum in the short wavelength region of VIS at 435. Two absorption peaks were detected at 669 and at 766 nm representing the Qy absorption band of BChl c and BChl a, respectively. The ratio of the absorbances of the red peaks of BChl c and BChl a was 4.979.

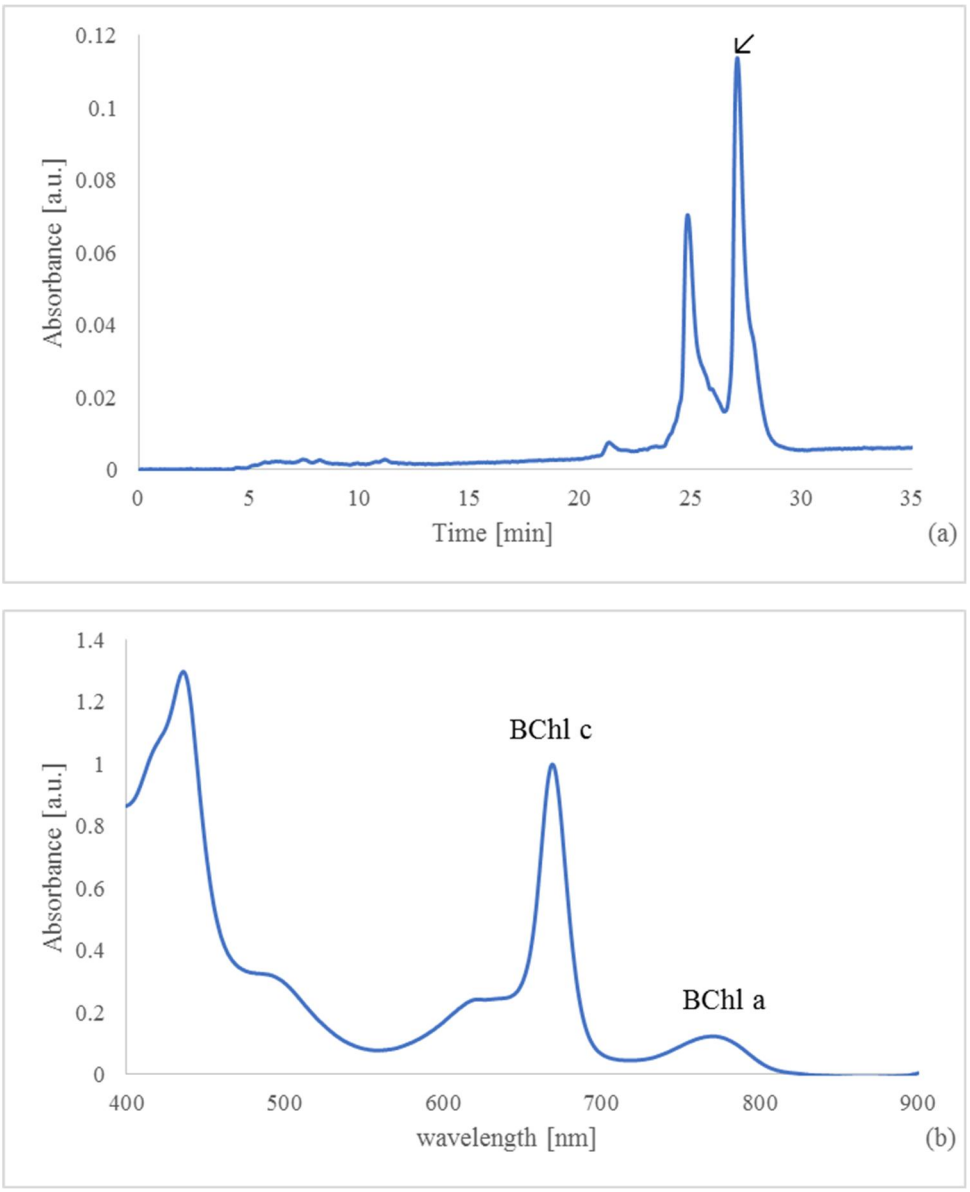

Figure 5. C5-Jupiter column pigment separation (a) chromatogram and (b) absorption spectrum (at 400-900nm range) of the main BChl c fraction (retention time 27min) captured by C5-Jupiter column.

Obtained results from column C8-Luna (flow of 3mL/min, pressure 16MPa and 20µl injection) are shown in Fig. 6. There are two major peaks in chromatogram at 30 min and 32 min (Fig. 6a). From the most intensive peak at 32min, absorption spectra were measured (Fig. 6b). Three peaks were observed at 438 nm and 671 nm and 764 nm. The absorption ratio for BChl c over BChl a at 671nm and 764 nm is 8.707.

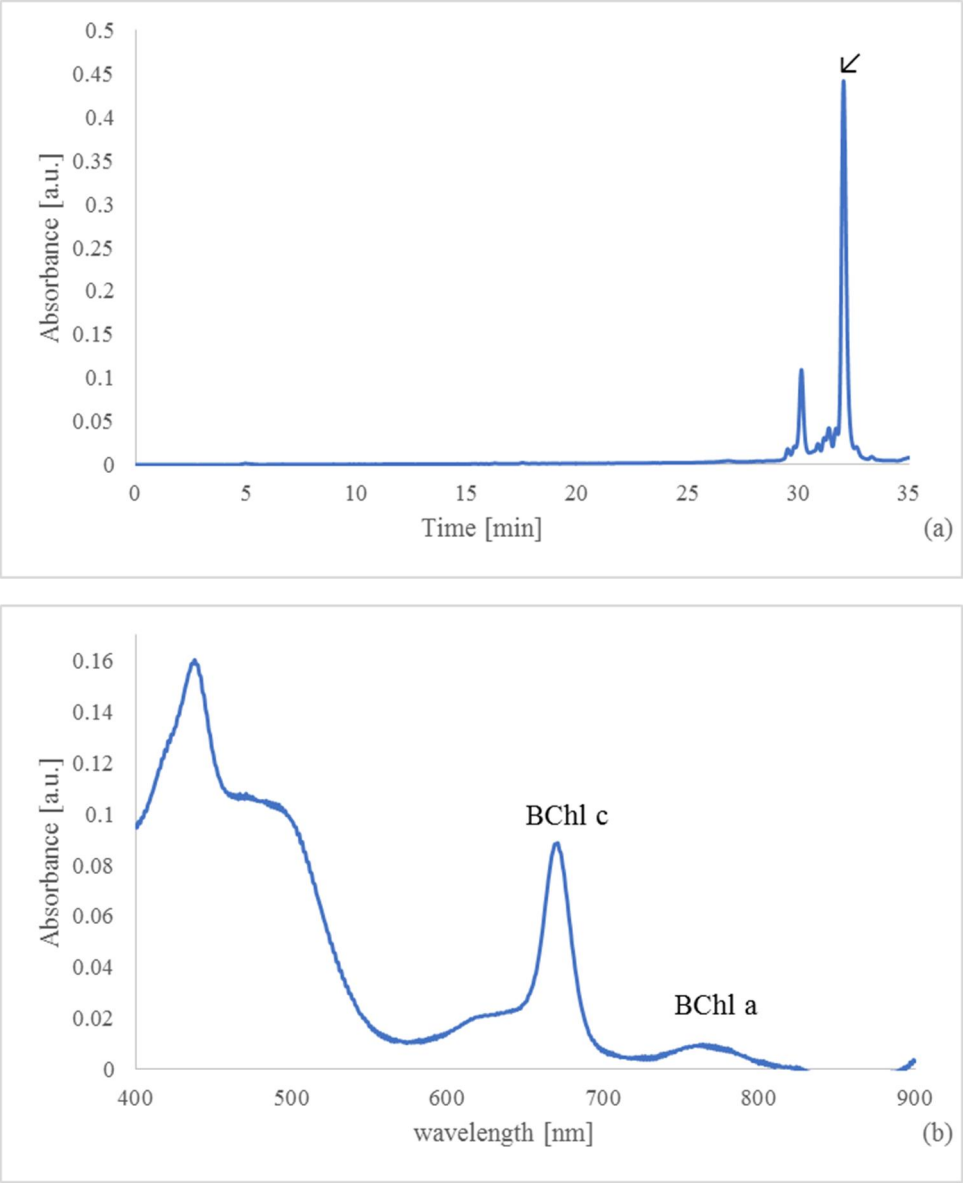

Figure 6. C8-Luna column pigment separation (a) chromatogram and (b) absorption spectrum (at 400-900nm range) of the main BChl c fraction (retention time 32 min) captured by C8-Luna column.

The separation using C8-Kinetex column is demonstrated in a chromatogram showing one major peak present at 32.5min and a minor peak is present at about 31 min (Fig. 7a). The major peak at 32.5min was collected and its absorption spectrum was taken. According to Figure 7b there are three peaks at 436nm, 669 nm and 769 nm. The absorption ratio for BChl c over BChl a at 669 nm and 769 nm is 8.133.

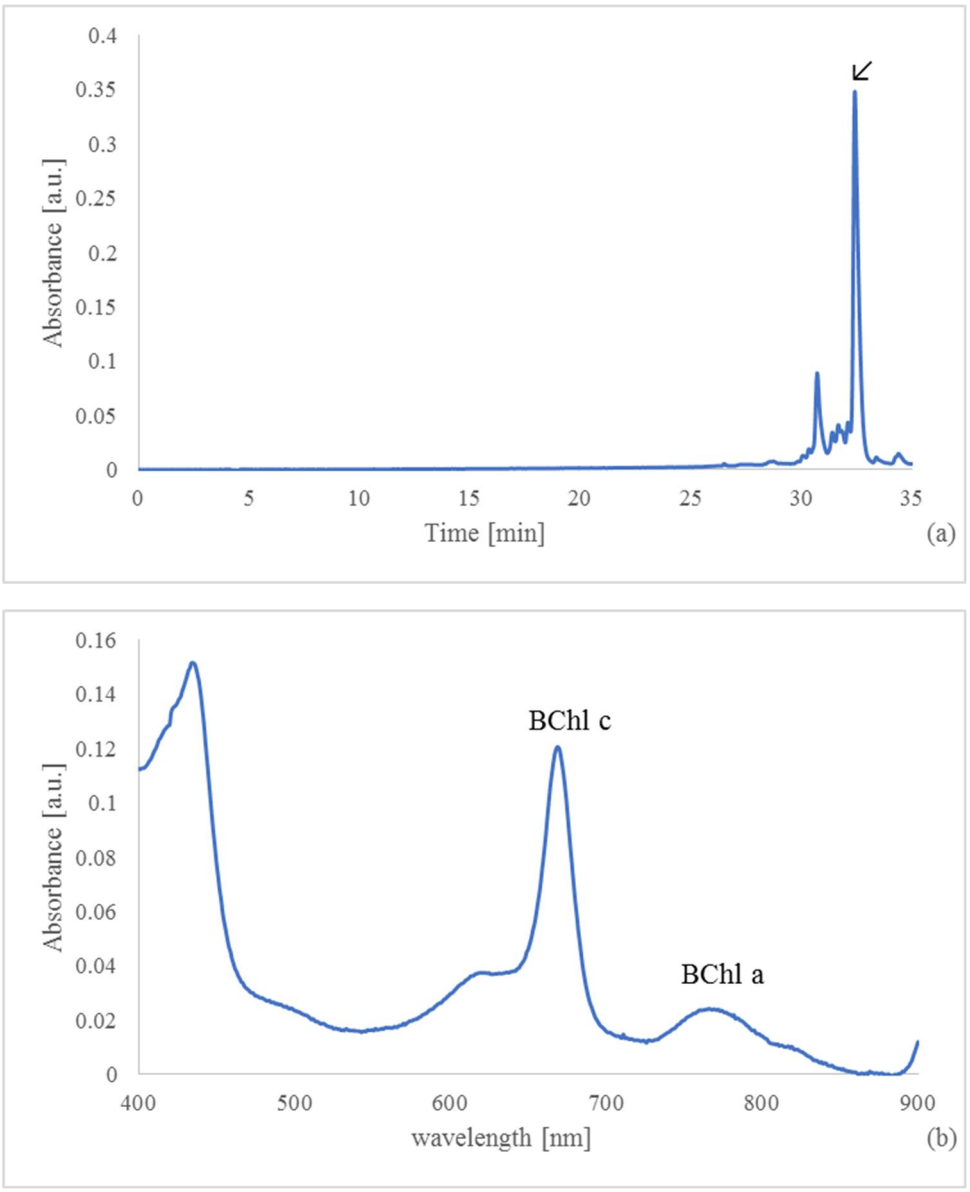

Figure 7. C8-Kinetex column pigment separation (a) chromatogram and (b) absorption spectrum (at 400-900nm range) of the main BChl c fraction (retention time 32.5 min) captured by C8-Kinetex column.

The comparison of the pigment extract separation using the three HPLC columns (C5-Jupiter, C8-Luna and C8-kinetex) is shown in Figure 8.

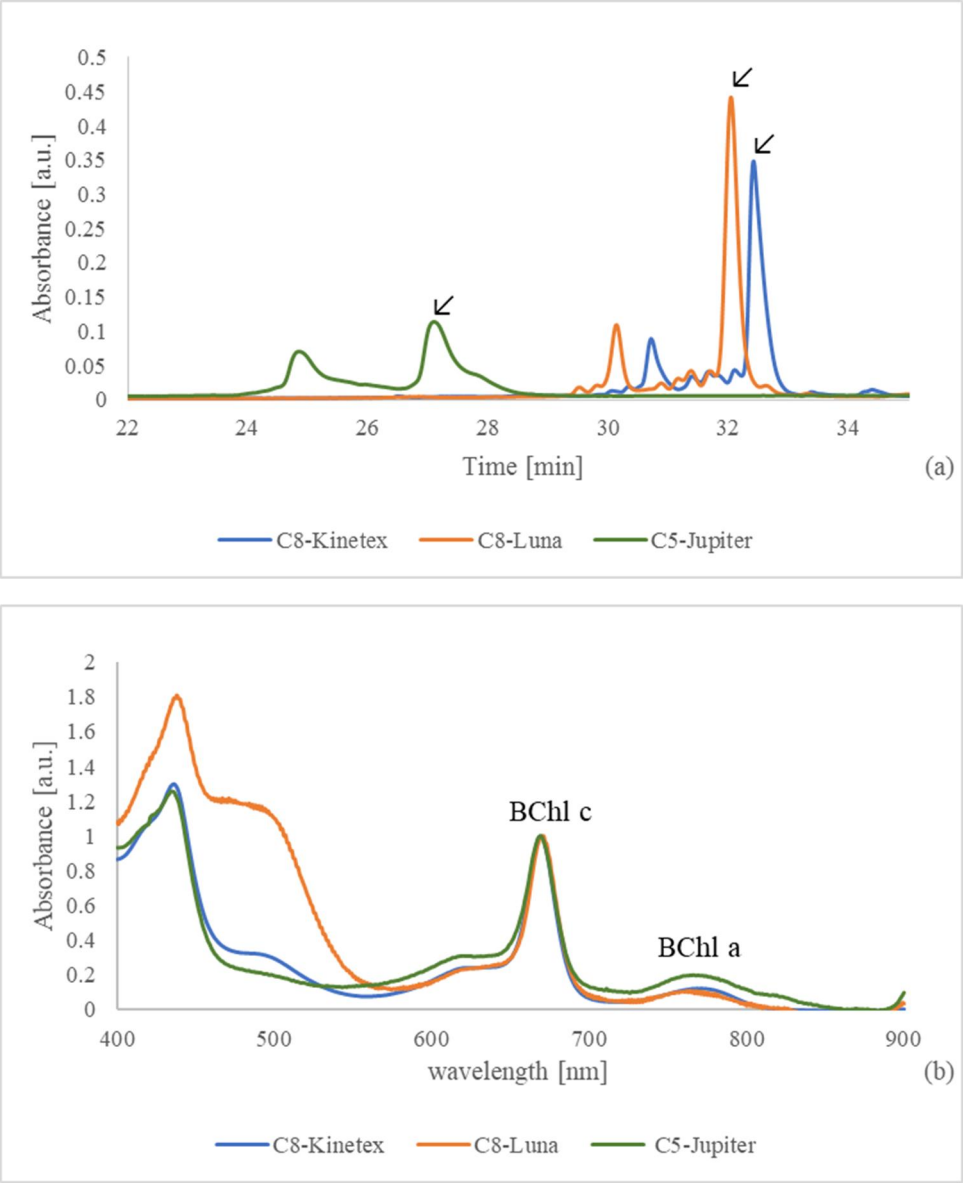

Figure 8. Comparison of three different columns (a) Chromatograms (b) absorption spectrum (at 400-900nm range). All spectra were normalized at maximum absorbance of BChl c.

4.4. Improved extraction of BChl c from cells

An innovated extraction procedure of BChl c from cells of *Cfl. aurantiacus* cells was devised. First, the non-polar solvents from the cell pigment extract (Acetone/Methanol/Tris 7:2:1 (v/v/v) solvent mixture) were removed by drying under vacuum in a rotary evaporator. Then, a more polar solvent than the acetone containing solvent formulation was used to extract the pigments. We chose LC-MS grade pure methanol to extract pigments from the dry pigment mixture. Methanol preferentially extracted the BChl c from the dry pigments leaving large fraction of BChl a behind, along with some carotenoids as visible in Figure 9.

The spectrum of the raw cell extract using Acetone/Methanol/Tris 7:2:1 (v/v/v) solvent mixture (Fig. 9 orange trace) and 100% methanol (Fig. 9 blue trace) extracted pigments are shown in Figure 9. Significant peaks of the raw extract are present at 436 nm (representing Soret band of BChl c) and 668.5 nm (representing BChl c Qy band). A smaller peak is also present at 342.5 nm that represents the Soret band of BChl a whereas the 768.5 nm peak corresponds to Qy of BChl a. Larger absorption in the infrared region (700-900) of the primary cell extract shows that BChl a was not extracted into methanol effectively.

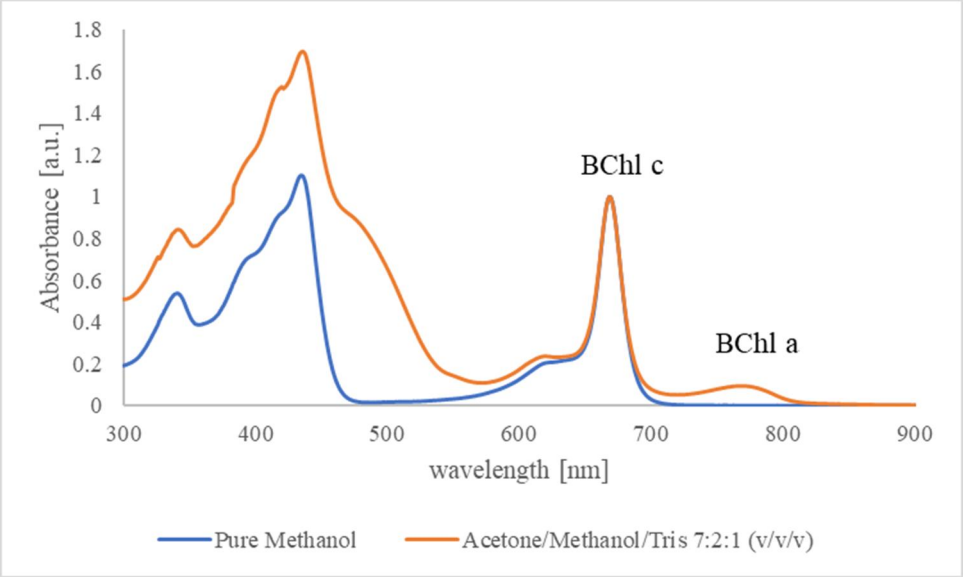

Figure 9. UV-VIS Spectrum (at 400-900nm range) of pigments extracted from whole cells of *Chloroflexus aurantiacus* using Acetone/Methanol/Tris 7:2:1 (v/v/v) solvent mixture and pure methanol.

4.5. Final HPLC purification step

Chromatogram of the pigments extracted to methanol that were loaded on C18-Kinetex column is shown in Figure 10. A single dominant peak appears at 9 min retention time, preceded by two minor peaks at 6 min and 8.5 min (Fig. 10a). The major peak was collected and its absorption spectrum was measured (Fig. 10b). The absorption spectrum of this fraction features two major peaks at 436 and 668.5 nm. Additional peak can be seen at the shoulder of the major red peak at 620nm. The ratio of BChl c over BChl a is 643.91.

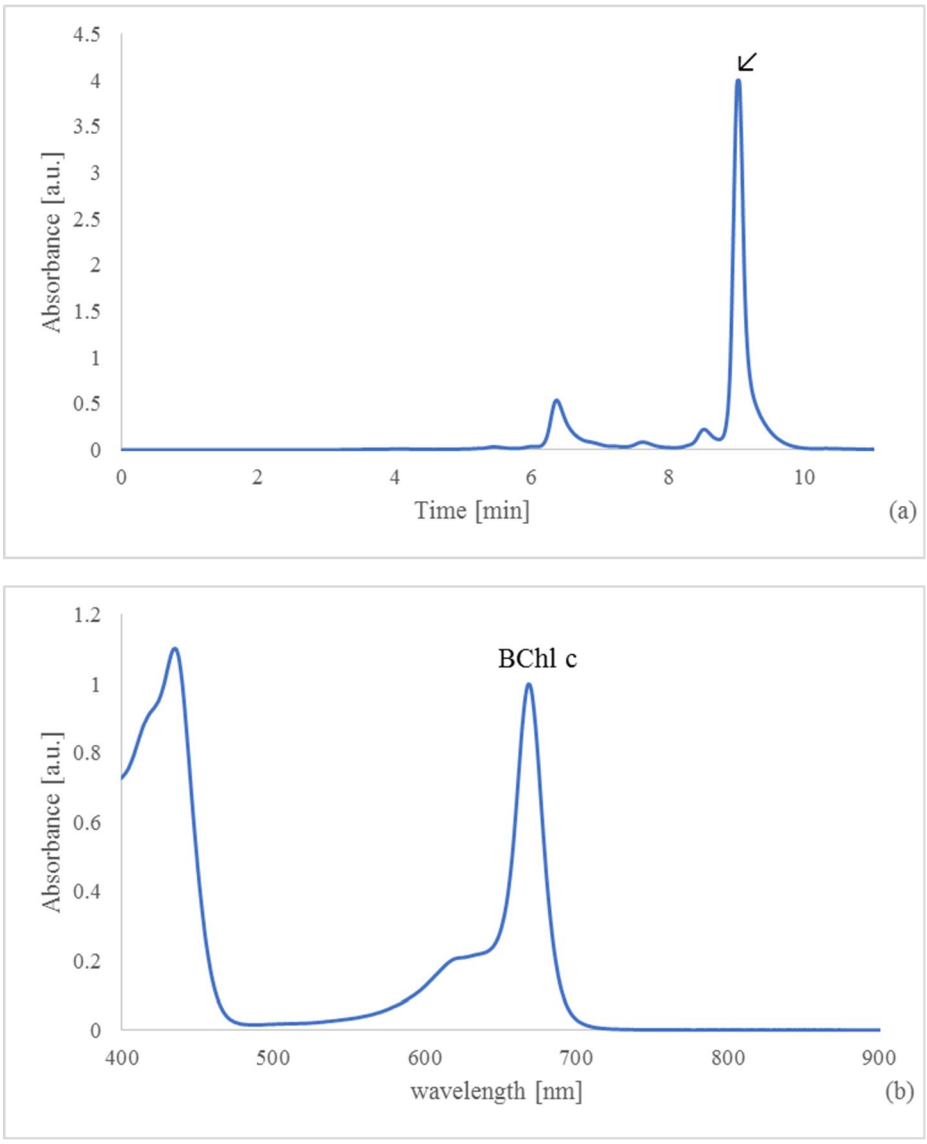

Figure 10. (a) chromatogram and (b) absorption spectrum (at 400-900nm range) captured from C18-kinetex column.

4.6. LC-PDA-APCI-MS/MS analysis of BChl c pigments

Firstly, two sets of chromatograms measured using PDA detector at 200, 300, 480 and 668 nm (Fig. 11) were analyzed. Identification of the chromatographic peak at 3.9 min, which belongs to the BChl c, was based on strong absorption at 668 nm and mass-to-charge ratio of its precursor ion (841.6 m/z). Then, full scan MS spectra of precursor ions in the peak of interest were compared. The MS spectrum of the extract before purification (Fig. 12) shows the signal of the BChl c, but the signal is not dominant and lots of other interfering signals are present in significant intensities. In contrast, MS spectrum of the extract after purification (Fig. 13) shows that the signal of the BChl c became the dominant signal of the MS spectrum. The increased concentration of the BChl c and the decrease in the concentration of co-eluting interferons in the extract after purification implies that our purification procedure was efficient. Finally, confirmation of the identity was

performed by comparing of MS/MS spectra of precursor ion (Fig. 14 and 15). Both MS/MS spectra show the same number of the same product ions, no product ion missing, pointing to the fact that the mass 841.6 m/z from the sample before purification represents signal of the same compound as the mass 841.6 m/z from the sample after purification. Different relative intensities of some product ions are probably caused by different matrix effects during fragmentation process in the course of measurement of MS/MS spectra.

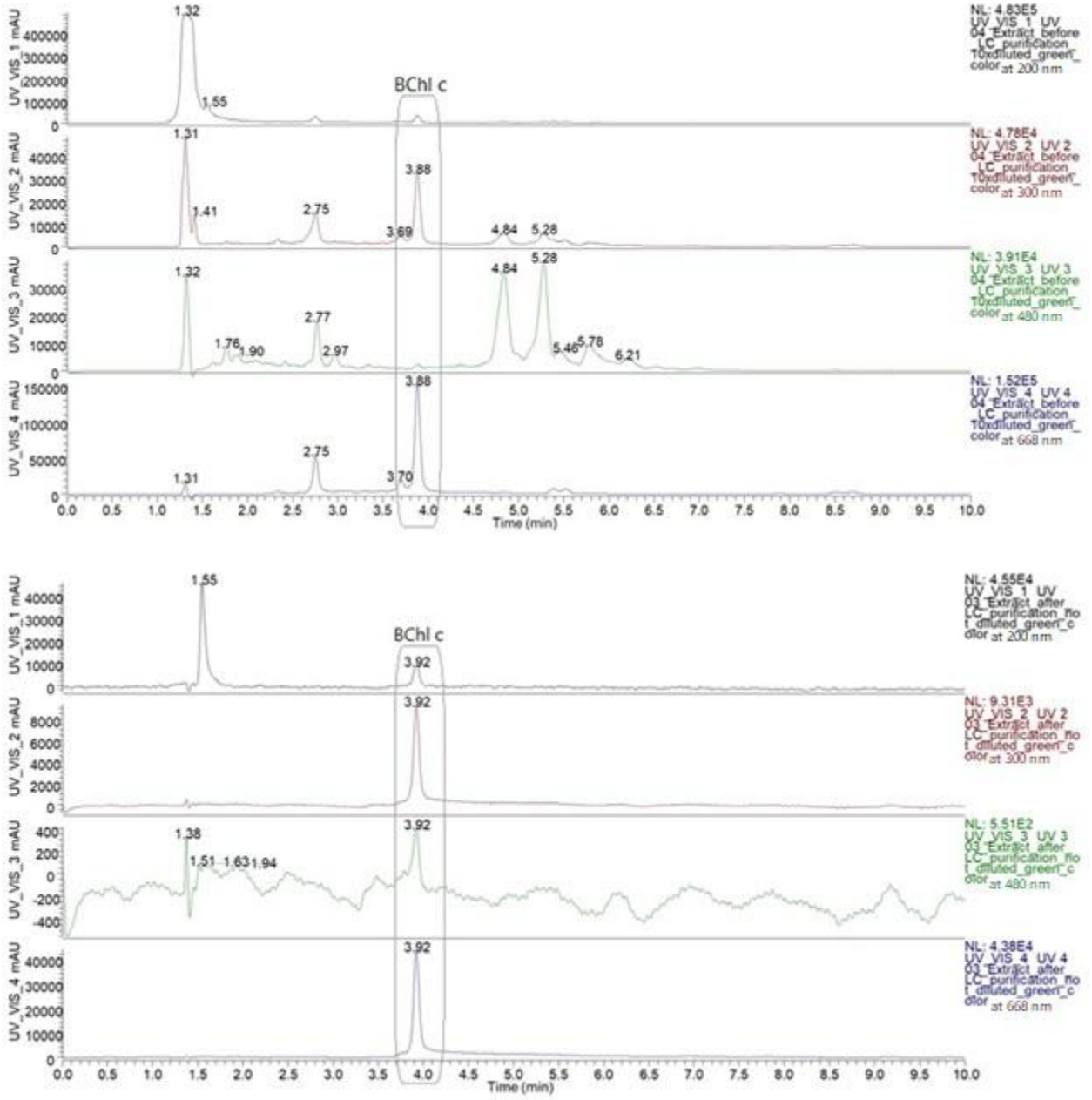

Figure 11. Chromatograms of the extract samples before purification (higher picture) and after purification (lower picture) measured using PDA detector at 200 nm (UV_VIS_1), 300 nm (UV_VIS_2), 480 nm (UV_VIS_3) and 668 nm (UV_VIS_4).

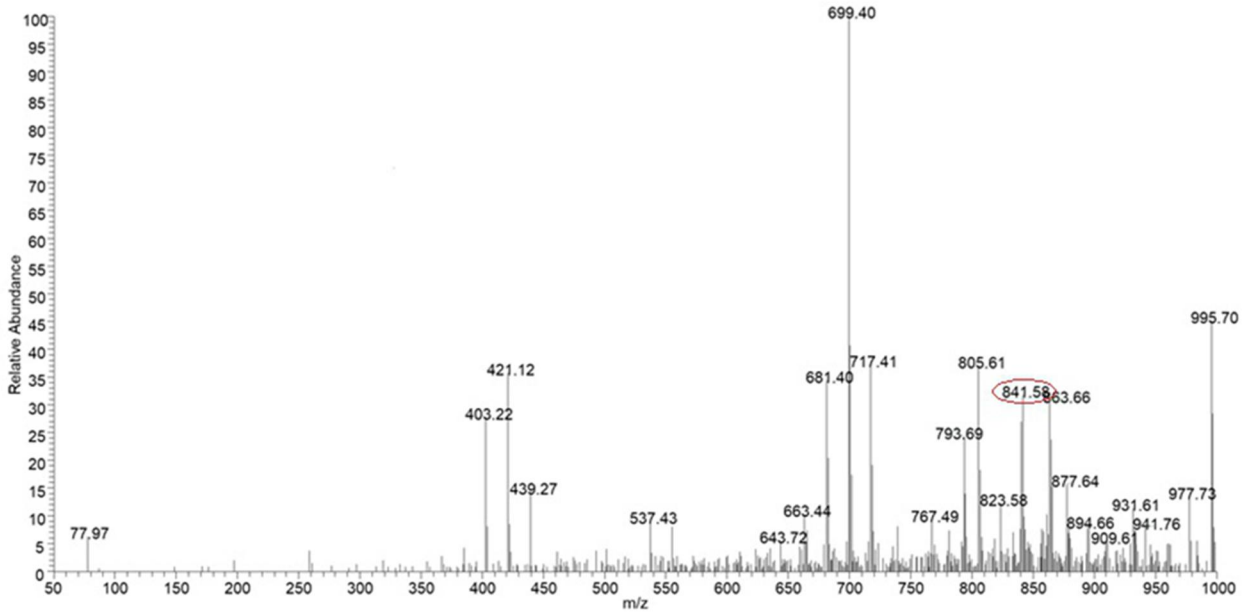

Figure 12. Full scan MS spectrum of precursor ions in the chromatographic peak of BChl c at retention time 3.9 minutes - the extract sample before purification.

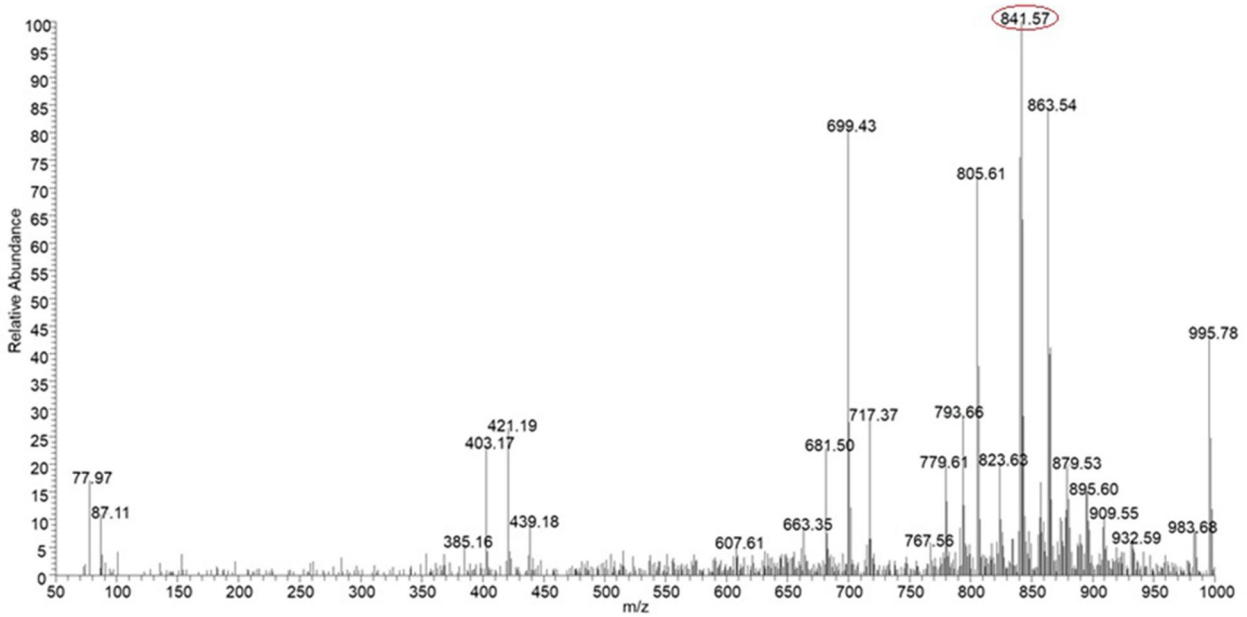

Figure 13. Full scan MS spectrum of precursor ions in the chromatographic peak of BChl c at retention time 3.9 minutes - the extract sample after purification.

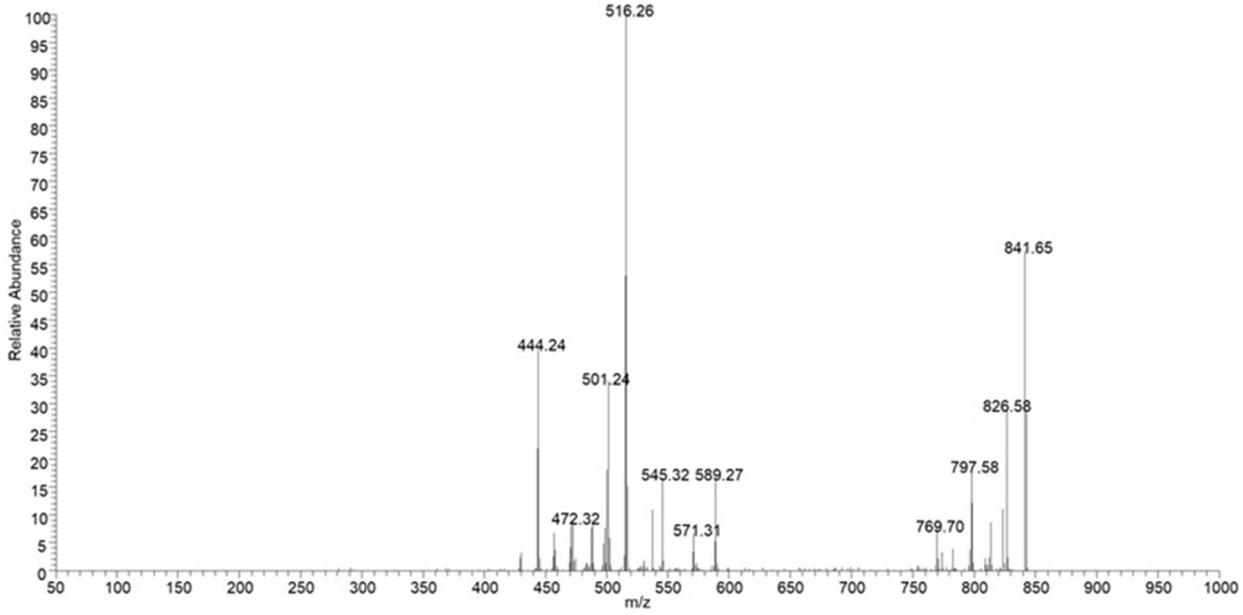

Figure 14. Full scan MS/MS spectrum of product ions obtained from the precursor ion of BChl c (841.6 m/z) - the extract sample before purification.

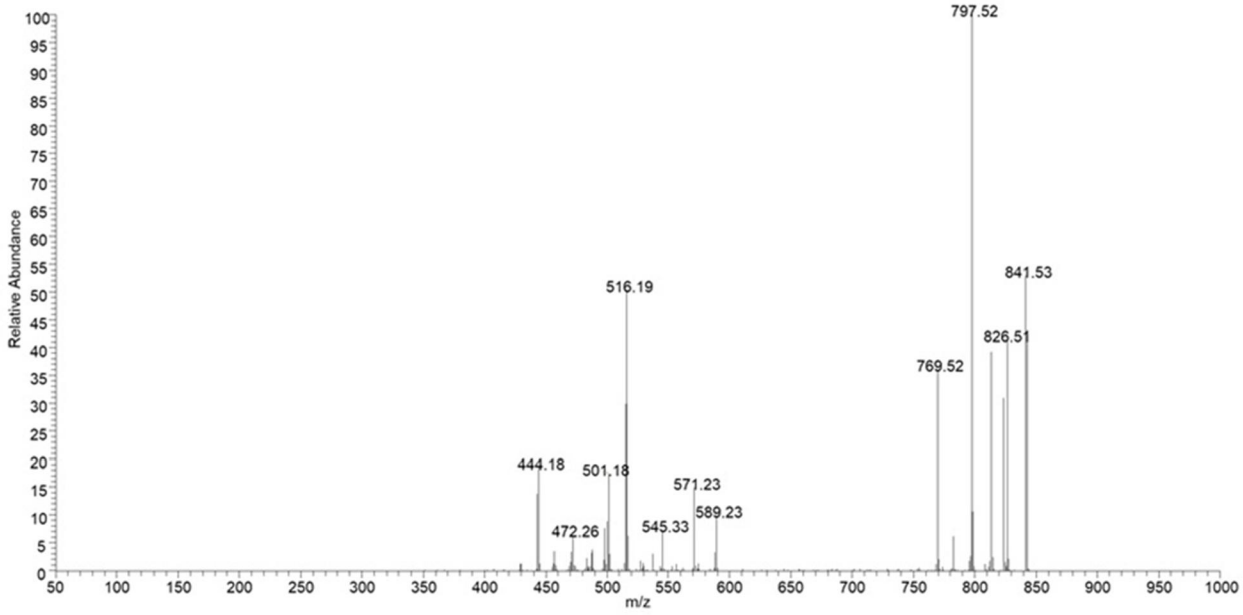

Figure 15. Full scan MS/MS spectrum of product ions obtained from the precursor ion of BChl c (841.6 m/z) - the extract sample after purification.

4.7. AFM imaging of BChl c aggregates

BChl c aggregates immobilized on HOPG were imaged by AFM using QI mode. Figure 16 shows a topography of the aggregates imaged in air having an ellipsoidal shape with a length of 150 nm and a width of 100 nm. AFM imaging in buffer reveals that aggregates of BChl c have dimensions 50×120×30, shape is rather round (show in Fig. 17) but sometimes polyhedral. Only gross structural features were observed. No fine details that would lead to elucidation of the spatial arrangement of the BChl c molecules forming the aggregate were detectable.

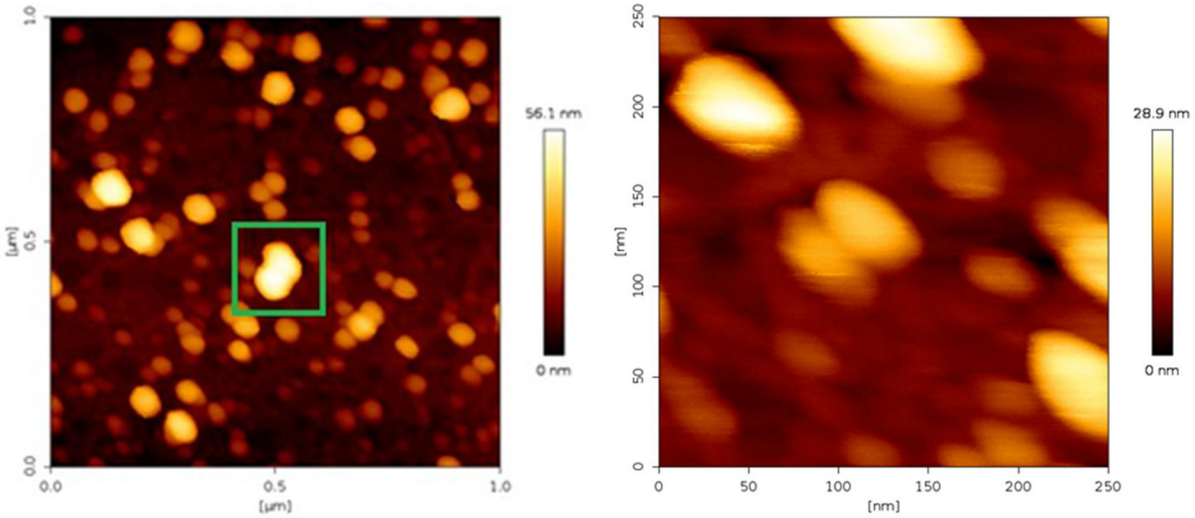

Figure 16. Aggregates on HOPG and zoomed in aggregates on HPOG, air.

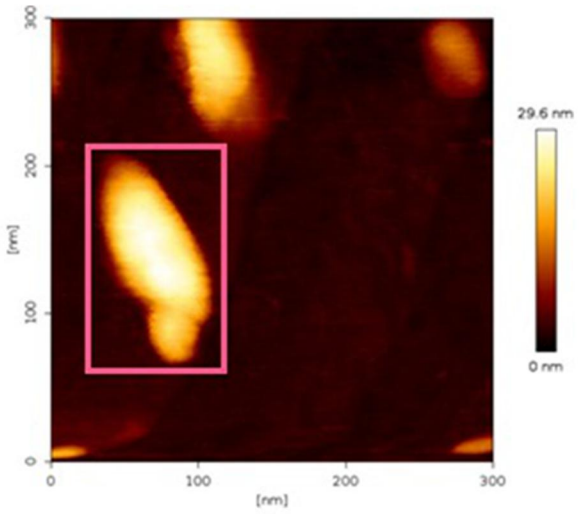

Figure 17. zoomed in aggregates on HPOG, buffer.

5. Discussion

The aim of this study was to optimize production and purification of the photosynthetic pigment of light harvesting antennae of green sulfur and nonsulfur photosynthetic bacteria BChl c. The pure pigment was utilized for production of BChl c aggregates that were imaged in AFM. High resolution imaging was attempted that would provide details of the spatial arrangement of the BChl c molecules in the aggregates. To achieve the set goals, cells of *Cfl. aurantiacus* were grown in a half strength of liquid R2A medium in medium scale batch cultures under anaerobic conditions and under light. The results of pigment analysis of cells grown in anaerobic conditions illustrate both BChl a and BChl c content in the absorption spectra. Separation of BChl c from the other pigments present in the cells was optimized by screening two protocols for pigment extraction, two protocols of reverse phase HPLC and four HPLC columns. The effectiveness of the final purification protocol for BChl c was confirmed by absorption spectroscopy and LC-MS.

To analyze the pigment composition, a mixture of the homogenized cells of *Chlorofelexus aurantiacus* and acetone: methanol: 50 mM Tris, pH 8 (7:2:1, v/v/v) was vortexed and then centrifuged. Afterwards, the cell debris containing unextracted pigments was separated from the supernatant containing the extracted pigments. The extracts were filtered and dried. All manipulations were done in the dark. Dried pigments were resuspended in 100% methanol. This procedure was similar to Psencík J. et al [38] study.

To separate the photosynthetic pigments, the particulate packing columns (C18 and C8) in the HPLC were mostly utilized [56- 58]. Moreover, to increase the quality of separation, the gradient technique was applied. In some HPLC procedures acetone has been utilized as the mobile phase [57, 59].

To distinguish the best method for separation and purification of BChl c were compared the performance of C5-Jupiter, C8-Luna and C8-Kinetex HPLC columns with gradient program. The injection volume in C8-Kinetex column was a half amount of the one in C5-Jupiter using the same protocol. This may be in part responsible for the obtained chromatograms show sharper and more intense peaks in C8-Kinetex column (illustrated in Fig. 8). The intensity of the chromatographic peaks eluted from C8-Luna are not considerably higher than the peaks recorded in C8-Kinetex chromatograms despite the injection volume for C8-Luna was a double amount of the sample loaded onto the C8-Kinetex column. The absorption spectrum of the collected fraction eluted from the C8-Kinetex column showed the least amount of BChl a and carotenoid in comparison to two other absorption spectra acquired using C5-Jupiter and C8-Luna columns. According to Figure 8, the Fraction of C8-Luna showed the highest peak of carotenoid and the lowest peak of BChl a (Qy band) whereas C5-jupiter shows the highest peak of BChl a (Qy band) and lower peak of carotenoid.

In improved method of purification, first, the cell pigment extract was dried under vacuum in a rotary evaporator to remove non-polar solvent. Then, a more polar solvent (LC-MS grade pure methanol) than the acetone containing solvent formulation was used to extract the pigments. The

BChl c was extracted by methanol while large fraction of BChl a was removed. In another procedure, hexane was used instead of methanol to extract carotenoids and BChl a. BChl c would stay on a side of the flask that could be then extracted by solvent that is less non-polar or one that is almost polar [60].

The separation with the HPLC columns featuring stationary phase functionalized with short hydrocarbon chains (C5, C8) resulted in only a partial success. C18-Kinetex columns with a more hydrophobic chains have a more reasonable function in the separation of isomers or other compounds with a similar structural and chemical properties [56]. These columns were shown to provide many advantages in the separation of the hydrophobic pigments [56]. Here we employed C18-Kinetex column (150×4.6 mm, 2.6 µm, 100 Å, Phenomenex) in an isocratic elution with pure methanol providing an acceptable procedure to purify BChl c [61]. The chromatographic separation using the C18-Kinetex column showed two major and numerous minor BChl c fractions. The second major band containing higher BChl c concentration exhibited absorption spectrum with two maxima at 435 nm and 668.5 nm that are remarkably similar to the two maxima at 434-435 nm and 669 nm obtained by Daniel C. Bruñe et al [15].

In this study, the substantially purified BChl c from *Cfl. aurantiacus* was analyzed by LCMS to confirm its high purity. The mass spectrum of the BChl c fraction exhibited a dominant mass of 841.6 m/z for molecular ion, which is the same findings as 840 m/z in Brune et al. [15]. The molecular weight predicted for stearyl-esterified, 4-ethyl-5-methyl substituted form of BChl c, which according to Gloe and Risch predominates in *Cfl. Aurantiacus* (1978) is 841.5g/mol It has been found that a majority of the *Chloroflexi* members did not methylate BChl c [62]. Thus, the greatest level of Qy absorbance of BChl c aggregates in the chlorosome of the organism can slightly be blue shifted with reference to *C. tepidum* and "*Ca. Chloracidobacterium thermophilum*" [62].

6. Conclusion

In this work, green non sulfur photosynthetic bacterium *Cfl. aurantiacus* was grown in a semi-continual, batch culture for production of BChls c pigment. Conditions for the growth were optimized yielding high yields of cells and BChl c under anaerobic conditions in light at 50˚C at light of 50 µmol photons m^{-2} s^{-1}. An efficient method for pigment extraction from the harvested cells was optimized for maximizing BChl c yields over the more nonpolar pigments – BChl a and carotenoids. This was achieved by two step extraction. The first step involved homogenization of the cells and extraction into a solvent mixture of acetone: methanol: 50 mM Tris, pH 8 (7:2:1, v/v/v). Second step involved drying the first extract and its subsequent extraction into a more polar methanol. This final pigment extract was purified using reverse phase HPLC column Kinetex C18. The BChl c fraction was purified using isocratic elution by methanol. The optimal chromatographic method is fast, efficient and uses only a single mobile phase that can be recycled for less demanding tasks e.g. SDS gel de-staining. The purity of the BChl c was confirmed by absorption spectroscopy and validated by LCMS and MS/MS. The purified BChl c was used in production of BChl aggregates using the method of alkane facilitated aggregation. The aggregates

formed by injecting of dichlormethane dissolved BChl c into hexane were immobilized on HOPG and imaged in AFM in air and also in aqueous solution. Unfortunately, the AFM imaging did not reveal any substructural details of the aggregates.

7. References

[1] Samokhvalov, P., Artemyev, M. et al. 2013. Basic principles and current trends in colloidal synthesis of highly luminescent semiconductor nanocrystals, Chem. Eur. J. 19, 1534-46.

[2] Sreekanth, K V., Zeng, S. et al. 2012. Excitation of surface electromagnetic waves in a graphene-based Bragg grating, Sci Rep 2 737.

[3] Kasap, S., Capper, P. 2007 Springer Handbook of Electronic and Photonic materials 2nd edition.

[4] Tadepalli, S., Slocik, J. M. 2017. Bio-Optics and Bio-Inspired Optical Materials. Chemical Reviews. 117 (20), 12705-63.

[5] Kolle, M., Lee, S. 2018. Progress and Opportunities in Soft Photonics and Biologically Inspired Optics". Advanced Materials. 30 (2), 1-40.

[6] Chen, W., Leykam, D., Chong, Y. D., & Yang, L. 2018. Nonreciprocity in synthetic photonic materials with nonlinearity. MRS Bulletin, 43(6), 443-451.

[7] Francis, G.W. 2000. PIGMENTS | Thin-Layer (Planar) Chromatography. Encyclopedia of Separation Science, 3839-50.

[8] Scheer, H. 2003. The pigments. In: Green B and Parson W (eds) Light-Harvesting Antennas in Photosynthesis, Kluwer Academic Publishers, Dordrecht, 29-81.

[9] Grimm B., Porra R.J. et al., 2006. Chlorophylls and Bacteriochlorophylls, Advances in Photosynthesis and Respiration 25, 1-25.

[10] Olson J.M. 1998. Chlorophyll organization and function in green photosynthetic bacteria. Photochem Photobiol 67, 61-75.

[11] van Rossum B.J., Steensgaard D.B. et al. 2001. A refined model of the chlorosomal antennae of the green bacterium Chlorobium tepidum from proton chemical shift constraints obtained with high-field 2D and 3D MAS NMR dipolar correlation spectroscopy. Biochemistry 40, 1587-95.

[12] Jochum, T., Reddy Ch.M. et al. 2008. The supramolecular organization of self-assembling chlorosomal bacteriochlorophyll c, d, or e mimics. Proc Natl Acad Sci USA 105, 12736-41.

[13] Umetsu, M., Wang, Zh. Y. 1999. How the formation process influences the structure of BChl c aggregates. Photosynthesis Research 60, 229-39.

[14] Blankenship R.E. et al. 1988. Energy Trapping and Electron Transfer in Chloroflexus Aurantiacus. In: Olson J.M., Ormerod J.G., Amesz J., Stackebrandt E., Trüper H.G. (eds) Green Photosynthetic Bacteria. Springer, Boston, MA, 57-68.

[15] Brune, D.C., Nozawa T. et al. 1987. Antenna organization in green photosynthetic bacteria. I. Organic bacteriochlorophyll c as a model for the 740 nm absorbing bacteriochlorophyll c in Chloroflexus aurantiacus chlorosomes. Biochemistry 26, 8644-52.

[16] Uehara, K., Olson, J.M. 1992. Aggregation of bacteriochlorophyll c homologs to dimer, tetramers and polymers in water-saturated carbon tetrachloride. Photosynth Res 33, 251-57.

[17] Tamiaki, H., Amakawa, M. et al. 1996. Synthetic zinc and magnesium chlorin aggregates as models for supramolecular antenna complexes in chlorosomes of green photosynthetic bacteria. Photochem Photobiol 63(1), 92-99.

[18] Nozawa, T., Ohtomo, K., et al. 1993. Structures and organization of bacteriochlorophyll c's in chlorosomes from a new thermophilic bacterium Chlorobium tepidum. Bull Chem Soc Jpn 66, 231-37.

[19] Balaban, T.S., Tamiaki, H. et al. 1997. Self-assembly of methyl zinc (31R)- and (31S)-bacteriopheophorbides d. J Phys Chem B 101, 3424-31.

[20] Chiefari, J., Griebenow, K. et al. 1995. Models for the pigment organization in the chlorosomes of photosynthetic bacteria: diastereoselective control of in-vitro bacteriochlorophyll cs aggregation. J Phys Chem 99, 1357-65.

[21] Smith, K.M., Craig, G.W. et al. 1983. Reversed-phase high-performance liquid chromatography and structural assignments of the bacteriochlorophylls-c*. Journal of Chromatography 281, 209-23.

[22] Umetsu M., Wang Z.Y. et al. 1999. Interaction of photosynthetic pigments with various organic solvents: Magnetic circular dichroism approach and application to chlorosomes, Biochimica et Biophysica Acta 1410, 19-31.

[23] Pierson, B.K., Cashtenholz, R.W. 1974. A phototrophic gliding filamentous bacterium of hot springs, Chloroflexus aurantiacus, gen. and sp. Nov. Arch. Microbiol 100, 5-24.

[24] Woese, C.R., Kandler, O., et al. 1990. Towards a natural system of organisms: proposal for the domains Archaea, Bacteria, and Eucarya, Proc. Natl. Acad. Sci. USA 87, 4576-79.

[25] Yamada, M., Zhang, H., et al. 2005. Structural and Spectroscopic Properties of a Reaction Center Complex from the Chlorosome-Lacking Filamentous Anoxygenic Phototrophic Bacterium Roseiflexus castenholzii. J Bacteriol 187(5), 1702-09.

[26] Feick, R.G., Fitzpatrick, M., et al. 1982. Isolation and characterization of cytoplasmic membrane from the green bacterium Chloroflexus aurantiacus. J. Bacteriol 150, 905-15.

[27] Tang, K.H., Urban, VS. et al. 2010. SANS investigation of the photosynthetic machinery of Chloroflexus aurantiacus. Biophys J 99, 2398-407.

[28] Blankenship, R.E., Matsuura, K. 2003. Antenna complexes from green photosynthetic bacteria. In Anoxygenic Photosynthetic Bacteria. Edited by: Green BR, Parson WW. Kluwer Academic Publishers, Dordrecht, 195-217.

[29] Tang, K.H., Wen, J. et al. 2009. Role of the AcsF Protein in Chloroflexus aurantiacus. J Bacteriol 191(11), 3580-87.

[30] Blankenship, R.E. 2002. Molecular Mechanisms of Photosynthesis, Blackwell Science Inc., Oxford, UK.

[31] Blankenship, R.E., Matsuura, K. .2003. in: Green, B.R., Parson, W.W., Light Harvesting Antennas in Photosynthesis, Kluwer Academic Publisher, Dordrecht, 195.

[32] Shoji, S., Mizoguchi, T. et al. 2013. Reconstruction of rod self-aggregates of natural bacteriochlorophylls-c from Chloroflexus aurantiacus. Chemical Physics Letters 578, 102-05.

[33] Blankenship, RE., Olson, JM. et al. 1995. Antenna complexes from green bacteria. In: Blankenship RE, Madigan, MT.et al. Anoxygenic Photosynthetic Bacteria, Kluwer Academic Publishers, Dordrecht, 399-435.

[34] Smith, K.M. 2003. in: Kadish, K.M. Smith, K.M. et al. Porphyrin Handbook 13, 157.

[35] Montaño, G.A., Wu, H.M., et al. 2003. Isolation and characterization of the B798 light-harvesting baseplate from the chlorosomes of Chloroflexus aurantiacus. Biochemistry 42, 10246-10251.

[36] Xin, Y., Lu, YK. et al. 2009. Purification, characterization and crystallization of menaquinol:fumarate oxidoreductase from the green filamentous photosynthetic bacterium Chloroflexus aurantiacus. Biochim Biophys Acta. 1787(2), 86-96.

[37] Staehelin, L.A., Golecki, J.R., et al. 1978. Visualization of the supramolecular architecture of chlorosomes (chlorobium type vesicles) in freeze-fractured cells of Chloroflexus aurantiacus. Springer. Arch. Microbiol. 119, 269-277.

[38] Psencík, J., Ikonen, TP., et al. 2004. Lamellar organization of pigments in chlorosomes, the light harvesting complexes of green photosynthetic bacteria. Biophysical Journal, 87(2), 1165-1172.

[39] Klatt, CG., Bryant, DA. et al. 2007. Comparative genomics provides evidence for the 3-hydroxypropionate autotrophic pathway in filamentous anoxygenic phototrophic bacteria and in hot spring microbial mats. Environ Microbiol 9, 2067-78.

[40] Feick, R.G., Fuller, R.C. 1984. Topography of the photosynthetic apparatus of Chloroflexus aurantiacus, Biochemistry 23, 3693-700.

[41] Hale, M.B., Blankenship, R.E., et al. 1983. Menaquinone is the sole quinone in the facultatively aerobic green photosynthetic bacterium Chloroflexus aurantiacus, Biochim. Biophys. Acta 723, 376-382.

[42] Xin, Y., Lu, Y.K., R. et al. 2009. Purification, characterization and crystallization of menaquinol:fumarate oxidoreductase from the green filamentous photosynthetic bacterium Chloroflexus aurantiacus, Biochimica et Biophysica Acta (BBA) – Bioenergetics 1782, 86-96.

[43] Strunecký, O., Kopejtka, K., et al. 2019. High diversity of thermophilic cyanobacteria in Rupite hot spring identified by microscopy, cultivation, single-cell PCR and amplicon sequencing. Extremophiles 23, 35-48.

[44] Yakovleva, A.G., Taisovaa, A.S. 2018. Estimation of the bacteriochlorophyll c oligomerisation extent in Chloroflexus aurantiacus chlorosomes by very low-frequency vibrations of the pigment molecules: A new approach. Biophys Chem. 240, 1-8.

[45] Martin M., Guiochon, G. 2005. Effects of high pressures in liquid chromatography. J. Chromatogr. A 1090 (1-2), 16-38.

[46] Vasconcellos, P., Rocha, G.O.D., et al. 2015. Chromatographic Techniques for Organic Analytes. Comprehensive Analytical Chemistry 70, 267-309.

[47] Fratamico, P. M., Annous, B. A. et al, 2009. Biofilms in the Food and Beverage Industries, 539-68.

[48] Moldoveanu, S.C., David, V., 2013. Retention Mechanisms in Different HPLC Types. Essentials in Modern HPLC Separations. 145-190.

[49] Buschow K.H. J., Cahn R. W. et al. 2001. Encyclopedia of Materials, 2001. Science and Technology (Second Edition), 1-5.

[50] Holmes-Hampton, G.P., Tong, W.H., et al. 2014. Chapter Fifteen - Biochemical and Biophysical Methods for Studying Mitochondrial Iron Metabolism. Methods in Enzymology 547, 275-307.

[51] Nanowizard AFM Handbook, version 2.2, 02/2009.

[52] Carstensa, T., Ispasb, A., et al. 2015. In situ scanning tunneling microscopy (STM), atomic force microscopy (AFM) and quartz crystal microbalance (EQCM) studies of the electrochemical deposition of tantalum in two different ionic liquids with the 1-butyl-1-methylpyrrolidinium cation. Electrochimica Acta 197, 374-87.

[53] Enevoldsen, GH., Pinto, HP. et al. 2008. Detailed scanning probe microscopy tip models determined from simultaneous atom-resolved AFM and STM studies of the TiO2(110) surface. Phys. Rev. B 78 (045416), 1-19.

[54] Omata, T., Murata, N. 1983. Preparation of Chlorophyll a, Chlorophyll b and Bacteriochlorophyll a by Column Chromatography with DEAE-Sepharose CL-6B and Sepharose CL-6B. Plant & Cell Physiol. 24(6), 1093-1100.

[55] Hutter, J.L., Bechhoffer, J. 1993. calibration of atomic-force microscope tips. Rev. Sci. Instrum. 64, 1868-1873.

[56] Hegazi, M.M., Ruzafa, A.P., et al. 1998. Separation and identification of chlorophylls and carotenoids from Caulerpa prolifera, Jania rubens and Padina pavonica by reversed-phase high-performance liquid chromatography. Journal of Chromatography A 829, 153-59.

[57] Canjura, F.L., Schwartz, S.J. 1991. Separation of chlorophyll compounds and their polar derivatives by high-performance liquid chromatography. Journal of Agricultural and Food Chemistry 39, 1102-05.

[58] Wright, S., Jeffrey, SW. et al. 1991. Improved HPLC method for the analysis of chlorophylls and carotenoids from marine phytoplankton. Marine Ecology Progress Series 77, 183-96.

[59] Gross, J. 1991. Pigments in vegetables: chlorophylls and carotenoids, 1st ed. Van Nostrand Reinhold, New York, 13-17.

[60] Indriatmokoa, Shioia, Y. et al. 2014. Separation of Photosynthetic Pigments by High-Performance Liquid Chromatography: Comparison of Column Performance, Mobile Phase, and Temperature. Procedia Chemistry 14, 202-10.

[61] Garcia Costas, A. M., Tsukatani, Y. et al. 2011. Identification of the Bacteriochlorophylls, Carotenoids, Quinones, Lipids, and Hopanoids of “Candidatus Chloracidobacterium thermophilum”. J. Bacteriol 194(5), 1158-68.

[62] Chew, A.G.M., Frigaard, N.U., et al. 2007. Bacteriochlorophyllide c C-8(2) and C-12(1) methyltransferases are essential for adaptation to low light in Chlorobaculum tepidum. J. Bacteriol. 189, 6176-6184.